



PERGAMON

Solid State Communications 113 (2000) 553–558

solid
state
communications

www.elsevier.com/locate/ssc

In situ Raman scattering studies of the amorphous and crystalline Si nanoparticles

A.A. Sirenko^{a,*}, J.R. Fox^a, I.A. Akimov^{a,b}, X.X. Xi^a, S. Ruvimov^c, Z. Liliental-Weber^c^aDepartment of Physics, The Pennsylvania State University, University Park, PA 16802, USA^bA.F. Ioffe Physico-Technical Institute, Russian Academy of Sciences, St Petersburg 194021, Russian Federation^cLawrence Berkeley Laboratory, Berkeley, CA 94720, USA

Received 10 September 1999; received in revised form 26 October 1999; accepted 24 November 1999 by J. Kuhl

Abstract

We report on in situ studies of the vibrational properties of Si nanoparticles and ultrathin layers grown by dc magnetron sputtering in ultrahigh vacuum on amorphous MgO and Ag buffer layers. The average thickness of the Si layers ranged from monolayer coverage up to 200 Å. Transmission electron microscopy has been used to determine size and shape of the Si nanoparticles. Changes in the phonon spectra of Si nanoparticles during the crystallization process have been studied by interference enhanced Raman scattering technique. Marked size-dependences in the phonon density of states and the relaxation of the \mathbf{k} -vector conservation with decrease in size of the Si nanoparticles have been detected. The transition between crystalline- and amorphous-like behavior takes place in the particles with an average number of Si atoms equal to $(7 \pm 2) \times 10^2$. © 2000 Elsevier Science Ltd. All rights reserved.

Keywords: A. Nanostructures; D. Phonons; E. Inelastic light scattering

1. Introduction

As the size of condensed matter systems is reduced in one or more dimensions to nanoscale levels, the electron and phonon states are influenced due to confinement. The discovery of visible luminescence at room temperature from porous Si [1,2] increased interest in the modification of electronic and vibrational properties of silicon nanocrystals. The prospect of realizing light-emitting devices stimulated intensive investigations of various nanometer-sized Si-based structures using different kinds of preparation methods [2–8]. Recent experimental studies of nanocrystalline Si (nc-Si) demonstrated substantial changes in the luminescence properties and electronic bands, which were attributed to quantum confinement caused by the restricted size of the particles and a breakdown of \mathbf{k} -vector conservation [9–12].

Phonon states are also modified in semiconductor nanostructures (or quantum dots) from those of the bulk. Theory predicts confinement of the optical and acoustic vibrations [13–15], which can be described macroscopically as being

due to a difference in the bulk dispersions and the dielectric properties of the nanoparticles and the surrounding media. This effect has been experimentally observed in a number of semiconductor nanostructures by means of Raman scattering [5,16,17,18,19,20]. However, previous Raman scattering studies were mostly focused on samples with Si particles within a matrix or with ligands, such as polycrystalline hydrogenated Si [5], Si-rich SiO₂ films [6], prepared by pulverizing bulk Si [7], porous Si [17–19,21], or Si prepared by thermal evaporation [22]. In these systems, the influence of a matrix or surface contamination on the phonon spectra cannot be neglected. Thus, in the analysis of the observed shifts and broadening of the optical phonon lines, it was difficult to distinguish between effects due to phonon confinement, modification of the surface states, and matrix-induced stress. While all the above mentioned effects are possible, the phonon states of *isolated* Si nanoparticles have been relatively unexplored experimentally and publications on in situ measurements of nc-Si are rare [23].

In this paper, we report on in situ Raman studies of ultra-small Si particles and thin films grown in ultrahigh vacuum (UHV). The phonon states of the Si nanoparticles free of chemisorbed species as well as changes induced by the

* Corresponding author.

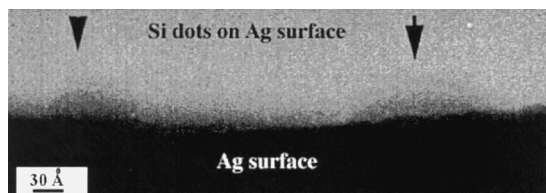


Fig. 1. TEM cross-section image of the recrystallized 30 Å sample grown on Ag buffer.

crystallization process and hydrogen termination will be discussed and vibration properties of the Si nanoparticles grown on dielectric and metallic substrates will be compared. Results of in situ electron energy loss spectroscopy (EELS) will be used for the characterization of the optical gap of Si nanoparticles.

2. Experiment

Ultrathin layers of Si were deposited on amorphous MgO or Ag buffers at room temperature by dc magnetron sputtering in a UHV chamber. A power of 6 W/cm² was applied to the Si sputter target. The background pressure of Ar was kept around 4 mTorr during the Si growth process. Before deposition of Si, the substrates were annealed at 500°C. The growth rate of Si, calibrated by both ex situ ellipsometry and profilometry, was about 0.5 Å/s. The average thickness of the Si layers, d , ranged from monolayer coverage up to 200 Å. In the following, the Si samples will be identified by their value of d . To crystallize Si ultrathin layers, the samples were heated up to about 500°C for 30 min in a UHV. The temperature of the sample was estimated by means of both a thermocouple attached to the sample holder and a pyrometer.

The grown ultrathin Si layers consist of nanometer-size clusters of a hemispherical shape formed on the substrate. Their average size and concentration varied with d . Ex situ transmission electron microscopy (TEM) was employed to characterize the shape and size of Si clusters in the samples grown on Ag buffer layers. Ag films with Si clusters were mechanically removed from the Si substrate, first, and then folded so that the Si clusters on the edge can be studied by TEM. Two Si clusters are seen in a cross-section image of the 30 Å sample annealed at 500°C (Fig. 1). The Si clusters in this sample have a 70–100 Å base width and are 30–40 Å high. The Si layer with a thickness of about 10, covers Ag buffer between quantum dots. These data are in a quantitative agreement with the calibrated average amount of deposited Si. Our results with in situ core-level X-ray photoemission (XPS) show that at $d \leq 50$ Å, Si forms nanoscale islands on MgO substrates as well. For thicker layers of Si, the characteristic MgO signal in the XPS spectra quickly disappears, corresponding to a complete coverage of the buffer-layer surface with Si atoms. We

determined that the Si clusters contain about $(70 \pm 20) \times d$ (Å) atoms for d less than 50 Å. For the samples with d more than 50 Å, no nanoparticle formation has been observed and their properties are the same as of thin films. It is similar to the growth regime of Ge nanoparticles with a hemispherical shape investigated previously with the same apparatus [24].

The Raman measurements were performed in situ at room temperature and at a pressure of 2×10^{-10} Torr in the UHV system. The main experimental problem in the system of two-dimensional composition of Si nanoparticles was a weak Raman signal due to extremely small scattering volume. For Si nanoparticles grown on MgO layers, we improved the situation by using interference enhanced Raman scattering (IERS) [25,26]. The Raman signal from the Si layer was increased by a factor of 10 in comparison with similar samples grown on Ag due to constructive interference in a bilayer structure. We found that in combination with multichannel detection [27], IERS can be sensitive even to a submonolayer coverage. Recently this technique provided useful information about the vibrations of surface and near-surface atoms of isolated Ge nanoparticles [24] and carbon nanocrystalline clusters and films [28]. In samples grown on MgO buffer-layers, the interference enhancement of the laser electric field close to the surface (the position of the Si layer) was achieved by utilizing a bilayer structure, which consists of a transparent dielectric film (MgO) deposited on a metallic layer (Ag) [25,26]. The entire structure was grown on a Si substrate. The thickness of the amorphous Ag, which works in a bilayer structure as a light reflector, was about 4000 Å. This is thick enough to screen completely any possible Raman signal from the Si substrate. The MgO thickness of 500 Å was calculated to give optimal interference enhancement at the exciting wavelength. The choice for the dielectric buffer layer (MgO) was determined by the two following reasons. First, the luminescence and Raman signal of MgO is weak at the green light excitation and, second, the analysis of the XPS spectra is easier than, e.g. in the case of a SiO₂ buffer, which also contains Si atoms.

Raman spectra were measured with a resolution of 0.8 cm⁻¹ using a SPEX Triplemate spectrometer equipped with a charge-coupled device (CCD) detector cooled with liquid nitrogen. The 5145 Å line (2.4 eV) of an Ar⁺-ion laser was used for excitation. The pumping power density was about 1 W/cm². Both the intensity and linear polarization of the Raman signal were analyzed in the conventional backscattering configuration (laser beam and scattered light are perpendicular to the sample plane). In the following, symbols VV and VH denote the scattering configurations with the polarization of the Raman signal being parallel and perpendicular to the polarization of the exciting beam, respectively. EELS spectra were measured with incident electron energy of 50 eV. An LK2000 spectrometer was operated with 5 eV pass energy yielding a resolution of approximately 0.03 eV.

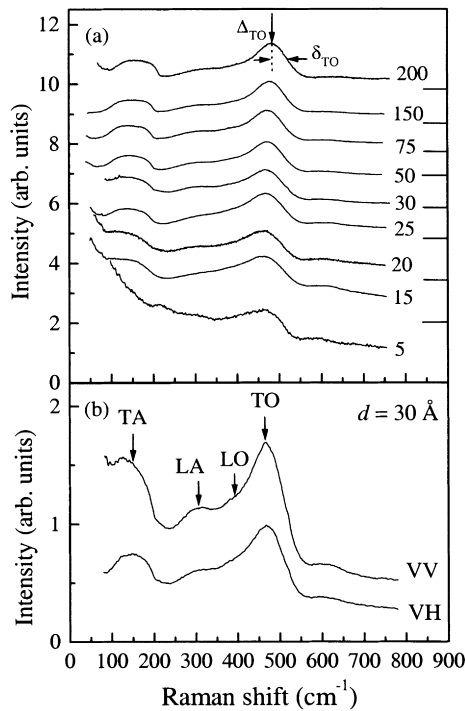


Fig. 2. (a) Normalized Raman spectra of amorphous Si layers measured with excitation at 2.4 eV. The respective average thicknesses are given next to the spectra in Å. The spectra were vertically shifted for clarity. The horizontal solid lines indicate the zero-signal levels. (b) Raman spectra of the 30 Å sample measured in VV and VH polarization.

3. Results and discussion

Raman spectra of amorphous samples with a different average thickness of the Si layer grown on MgO are shown in Fig. 2(a). As expected, the spectra of the relatively thick layers are similar to that of amorphous Si (a-Si) and consist of the TA, LA, and TO strong bands centered around 150, 310 and 480 cm, respectively, and the weak LO shoulder at 370 cm⁻¹ [29–31], marked in Fig. 2(b). The Raman spectra are polarized at the linearly polarized excitation. The VV and VH spectra are shown in Fig. 2(b) for the 30 Å sample. The degree of linear polarization, defined as $(I_{VV} - I_{VH}) / (I_{VV} + I_{VH})$, is about 0.25, which is close to the value previously determined for a-Si [32]. I_{VV} and I_{VH} are the Raman intensities in the corresponding configuration.

As the Si layer thickness decreases, the high frequency half-width-at-half-maximum (HWHM) of the TO band δ_{TO} defined as shown in Fig. 2(a) changes from 35 to 50 cm⁻¹. At the same time, the position of the maximum Δ_{TO} moves towards the low Raman shifts. The dependences of Δ_{TO} and δ_{TO} on d are presented in Fig. 3 for samples grown on both MgO and Ag. The observed broadening of the optical band in the Raman spectra of Si layers corresponds to the modification of the phonon density of states due to changes in the

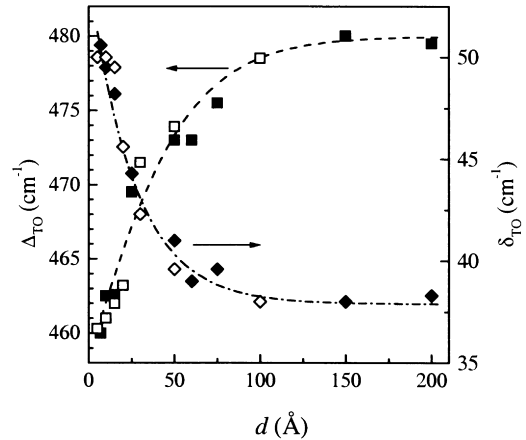


Fig. 3. The HWHM δ_{TO} and position Δ_{TO} of the TO Raman peak as functions of the average thickness of the amorphous Si layers. Closed and open symbols correspond to samples grown on MgO and Ag, respectively. Dashed lines guide the eye.

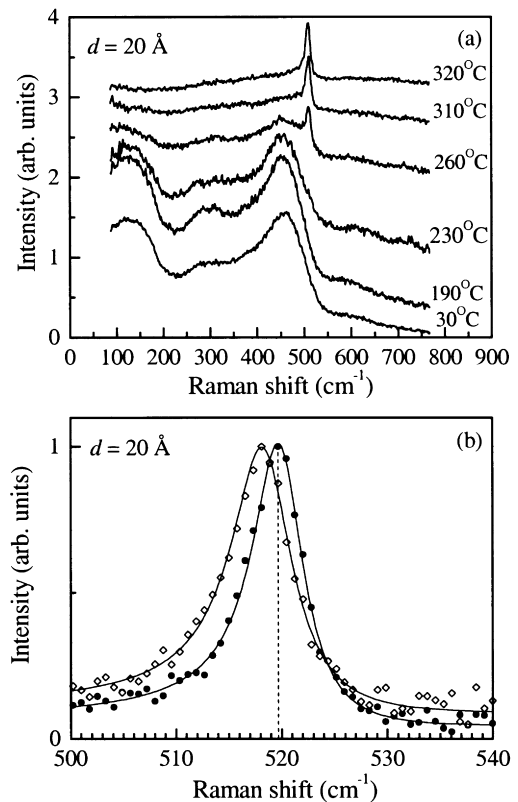


Fig. 4. (a) Normalized Raman spectra of the 20 Å sample measured at different temperatures during crystallization process. (b) Spectra of the $k=0$ optical phonon in the same sample before (open circles) and after termination of the surface with a hydrogen plasma (closed circles). Vertical dashed line shows a position of the c-Si (100) phonon [35] at 519.7 ± 0.8 cm⁻¹.

angular distribution of the sp-bonds in the near-surface atomic layers and dangling bonds on the surface [24,32]. The surface effects are expected to be more pronounced in ultrathin Si layers consisting of amorphous clusters, where a fraction of the surface atoms to interior atoms increases significantly. Indeed, the significant variation in the phonon spectra occurs for d less than 50 Å, the same thickness-range where the formation of the Si clusters was observed. In the case of relatively thick layers with $d \geq 50$ Å, any possible corrugation of the Si surface ($\Delta d = \pm 10$ Å) should not significantly affect the Raman spectra, which are similar to that of the a-Si films. Note, that in the samples grown on MgO buffer layers, formation of the Si–O bonds at the interface could lead to the similar transformation in the Raman spectra, especially in the ultrathin layers, where the fraction of the surface atoms is high. However, the thickness dependences of the optical band for the samples grown on both MgO and Ag were identical (see Fig. 3). Thus, we conclude that the vibration properties of the amorphous Si nanoparticles are determined by the size effects. Our experiments are also important to distinguish between size-dependent modifications of the phonon density of states from that due to contamination of the Si surface with hydrogen or oxygen. The latter might be neglected for our samples, but could be very strong in, e.g. porous Si.

After heating the samples, a remarkable transformation in the Raman spectra was observed. Fig. 4(a) shows several spectra for the 20 Å sample taken at different temperatures. The sharp crystalline peak arises when the temperature increases to more than $T \approx 260^\circ\text{C}$. Note the temperature-induced red shift of this Raman line. At the same time, the intensity of the amorphous-like broad features decreases at $T > 320^\circ\text{C}$. This indicates a partial recovering of the \mathbf{k} -vector conservation condition with crystallization of the Si layers allowing only scattering by optical phonons at the zone center ($\mathbf{k} = 0$), where the TO and LO phonons in bulk crystalline Si (c-Si) are degenerate [33]. The degree of linear polarization of this peak is about 0.16, which corresponds to the random orientation of the crystallographic directions in the Si nanoparticles. The crystallization temperature was found to be around 250–300°C for samples grown on both MgO and Ag (note that the crystallization temperature for a-Si films varies in a wide range depending on the sample preparation condition and substrates, see, e.g. Ref. [34]).

The position of the $\mathbf{k} = 0$ peak does not change significantly in different recrystallized samples. Its shape is asymmetric and a full-width-at-half-maximum (FWHM) varies from 6 cm^{-1} for thick layers to about 8 cm^{-1} (see Fig.4(b)) for 20 Å sample. For $d \leq 50$ Å, the typical red shift of this line with respect to the position of c-Si (100) phonon (the room temperature value for the $\mathbf{k} = 0$ phonon in c-Si varies in literature between 519 and 522 cm^{-1} , see, e.g. Refs. [35]) is about $1.5 \pm 0.5 \text{ cm}^{-1}$. From the first glance, this shift could be attributed to the phonon confinement. However, after termination of the sample surface with a hydrogen

plasma, the position of the $\mathbf{k} = 0$ peak shifts back and coincides within our experimental accuracy with the c-Si (100) phonon. The measurements were taken with the same pumping power and the heating effect was excluded. Thus, we conclude that the initially observed red shift of about 1.5 cm^{-1} is determined not by confinement of the optical phonons but is mostly due to the surface strain. In passivated recrystallized samples, hydrogen reduces the strain at the nanoparticle surface by destroying unfavorable tensile-strained Si–Si bonds [36]. A slight decrease in the FWHM of the Raman line (see Fig.4(b)) can be also due to this effect. Further we will briefly discuss effects, which can influence the position of the phonon lines in the Raman spectra of nanocrystals of intermediate size. After that we will proceed to the case of ultrasmall crystalline particles.

The absence of the confinement-induced shift of the optical phonon in the samples with d between 20 and 50 Å lacks a straightforward interpretation. On one hand, a simple estimation of the confinement-induced frequency shift of the optical phonon in a hemispherical particle [15] results in a value of about 5 cm^{-1} for the sample with $d = 20$ Å, which should be measurable with our experimental accuracy. On the other hand, there are several factors, which can strongly affect this simple picture decreasing the expected confinement-induced effect below our experimental limits:

1. The wide size distribution of the nanoparticles, which can result in a preferable excitation of the quantum dots with the maximum size increasing the average size of the dots, which are probed in the Raman experiments.
2. The inhomogeneous broadening of the Raman line, which is caused by the higher-order confined modes with the frequencies lower than the primary confined Raman line [37] and by the splitting between TO and LO phonons.
3. The strain between the dots and the substrate [5,7]. Note that the compressive strain shifts the line position in the opposite direction to that induced by confinement.
4. An increase of the fraction of the surface to interior atoms in smaller nanoparticles, leading to modification of the phonon density of states [28,32]. Note that the contribution of the surface vibrations may affect the Raman spectrum as well [38].

The combination of the above-mentioned factors, in principle, could be responsible for the fact that in the studied Si clusters, which contain only a few 1000 atoms, no strong systematic shift of the $\mathbf{k} = 0$ peak was detected. A comparison of higher resolution Raman measurements with precise theoretical investigation of the phonon confinement, which should take into account the exact shape of the nanoparticles (see Fig. 1), surface effects, and interaction with substrate, are required to clarify the situation. At this point we can only mention that our data are more similar to results for phonon confinement in thin Si films, where the relatively small Raman shifts were observed [15], and to specific cases of porous Si [39].

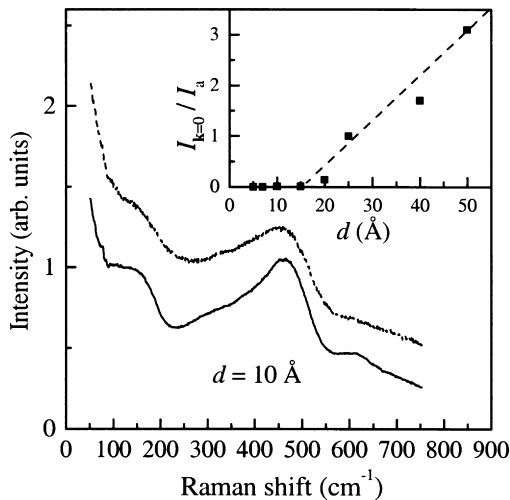


Fig. 5. Raman spectra of the 10 Å sample before (solid line) and after the annealing (dashed line). Inset shows the ratio of the $\mathbf{k} = 0$ peak intensity $I_{\mathbf{k}=0}$ to that of the amorphous background I_a as a function of the average thickness of the Si layers.

Nevertheless, in the ultrathin recrystallized Si layers, we expected a formation of much smaller Si clusters with a typical size of 10–30 Å, where the effect of the phonon confinement should become dominant. However, instead of a larger red shift of the phonon line, the $\mathbf{k} = 0$ peak disappeared in samples with $d \leq 10$ Å. As the average thickness of the Si layer decreases, the relative intensity of the $\mathbf{k} = 0$ peak to the intensity of the amorphous-like broad peak at 480 cm^{-1} becomes smaller. The ratio of the $\mathbf{k} = 0$ peak intensity to the amorphous-like background intensity is

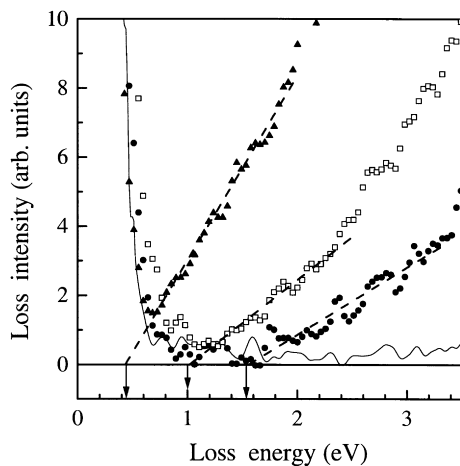


Fig. 6. EELS spectra of the 5 Å sample before (triangles) and after the annealing (circles). Dashed lines guide the eye to the onset of the electronic transitions indicated with arrows. Spectra for polycrystalline Si and SiO_2 are shown for comparison with open squares and solid line, respectively.

shown in inset to Fig. 5. In the case of the relatively thick films, with d greater than 45 Å, the complete \mathbf{k} -vector conservation could be achieved after annealing, which manifests itself by the vanishing of the amorphous-like features in the Raman spectra. In contrast, for Si layers with d less than 10 Å, the Raman spectra do not change with annealing and practically no modifications have been observed even after heating up to 600°C for 1 h. Two corresponding spectra of the 10 Å sample grown on a Ag buffer layer and measured at room temperature before and after annealing are shown in Fig. 5. This result is in agreement with the earlier prediction [32] and experimental observations [23,38,40] of the fact, that in ultrasmall nanocrystals the $\mathbf{k} = 0$ line vanishes and Raman spectra of both covalent and ionic nanocrystals become amorphous-like when they are small enough. Two reasons can be adduced to explain this effect. First, even in the ideal case of isolated nanocrystal, the decrease in size breaks the crystal periodicity allowing observation of the scattering from entire branches of the acoustic and optical phonons. The situation becomes similar to a system of weakly interacting molecules in liquids or gases and the consideration of \mathbf{k} -vector conservation becomes needless. Second, the fraction of disordered surface atoms increases with respect to the ordered atoms within a crystalline lattice [28,32]. The observed size-dependent modification of the Raman spectra is important for determination of the minimum size of a crystalline system, which can satisfy \mathbf{k} -vector conservation conditions. According to the aforementioned empirical relation between d and the average size of the nanoparticles, the transition between crystalline- and amorphous-like behavior takes place in the recrystallized samples with an average number of Si atoms in one hemispherical particle equal to $(7 \pm 2) \times 10^2$.

To support this statement an additional verification of the crystalline structure of the ultrasmall nanoparticles is required. Note, that one of the alternative explanations of the observed effect can be an increase of the temperature of the amorphous-to-crystalline structural transition. However, our in situ measurements of electron energy losses demonstrate significant modification of the electronic gap with annealing in the same temperature range, confirming that the structure of the annealed Si nanoparticles is *crystalline*. The EELS spectra obtained before and after recrystallization for a $d = 5$ Å sample grown on SiO_2 are shown in Fig. 6. The intensity was normalized to the elastic peak amplitude. The onsets of electronic transitions (shown with arrows in Fig. 6) in the amorphous sample occurs at much lower energy (0.45 ± 0.05 eV) than that seen in the annealed sample (1.55 ± 0.05 eV, similar values for the optical gap can be extracted from the EELS spectra by computing the absorption coefficient and using analogous techniques as those employed to amorphous semiconductors, for more detail see Ref. [41]). The latter value is much higher than the indirect gap of bulk crystals [42], which provides a clear evidence of the electron confinement in ultrasmall

nanocrystals. The observed increase in the electronic gap is in a good agreement with the recently reported changes in the band ages of silicon nanocrystals by X-ray absorption and photoemission [11].

4. Conclusions

The phonon states of Si nanoparticles free of chemisorbed species, which were grown and measured in ultrahigh vacuum, have been studied. Remarkable transformation in the phonon density of states with decrease in size of amorphous Si nanoparticles was observed. It has been found that the surface strain induced by the dangling bonds can result in a red shift of the optical phonon frequency for relatively big nanocrystals. We consider the observed relaxation of the \mathbf{k} -vector conservation in ultrasmall nanocrystals as the most important result of this paper. The average number of Si atoms per one particle, which corresponds to the transition between crystalline- and amorphous-like behavior, has been determined. A confinement-induced increase in the electronic gap of ultrasmall Si particles has been measured by means of in situ EELS providing a clear evidence of their crystalline structure.

Acknowledgements

The authors are grateful to V.I. Merkulov for useful discussions. This work was supported by USDOE Grant DE-FG02-84ER45095 and NSF Grant DMR-96-23315.

References

- [1] A.G. Cullis, L.T. Canham, *Nature (London)* 353 (1991) 353.
- [2] A.G. Cullis, L.T. Canham, P.D.J. Calcott, *J. Appl. Phys.* 82 (1997) 909 and references therein.
- [3] R. Tsu, J. Morais, Bowhill, in: Z. Feng, R. Tsu (Eds.), *Porous Silicon*, World Scientific, Singapore, 1994, p. 443.
- [4] K. Eberl, K. Brunner, W. Winter, *Thin Solid Films* 294 (1997) 98.
- [5] Z. Iqbal, S. Veprek, A.P. Webb, P. Capezzuto, *Solid State Commun.* 37 (1981) 993.
- [6] E.W. Forsythe, E.A. Whittaker, F.H. Pollak, S.W. Sywe, G.S. Tompa, B.A. Khan, J. Khurgin, H.W.H. Lee, F. Adar, H. Schaffer, in: R.W. Collins (Ed.), *Microcrystalline and Nanocrystalline Semiconductors*, Materials Research Society Symposia Proceedings No. 358MRS, Pittsburgh, 1994, p. 187.
- [7] X.S. Zhao, Y.R. Ge, J. Schroeder, P.D. Persants, *Appl. Phys. Lett.* 65 (1994) 2033.
- [8] L. Tsybeskov, *MRS Bull.* 23 (4) (1998) 33 and references therein.
- [9] W.L. Wilson, P.F. Szajowski, L.E. Brus, *Science* 262 (1993) 1242.
- [10] S. Schlupper, S.L. Friedman, M.A. Marcus, D.L. Adler, Y.-H. Xie, F.M. Ross, T.D. Harris, W.L. Brown, Y.J. Chabal, L.E. Brus, P.H. Citrin, *Phys. Rev. Lett.* 72 (1994) 2648.
- [11] T. van Buuren, L.N. Dinh, L.L. Chase, W.J. Siekhaus, L.J. Terminello, *Phys. Rev. Lett.* 80 (1998) 3803.
- [12] D. Kovalev, H. Heckler, M. Ben-Chorin, G. Polisski, M. Schwartzkopff, F. Koch, *Phys. Rev. Lett.* 81 (1998) 2803.
- [13] R. Alben, D. Weaire, J.E. Smith Jr., M.H. Brodsky, *Phys. Rev. B* 11 (1975) 2271.
- [14] T. Takagahara, *J. Lumin.* 70 (1996) 129.
- [15] I.H. Campbell, P.M. Fauchet, *Solid State Commun.* 58 (1986) 739.
- [16] A. Ekimov, *J. Lumin.* 70 (1996) 1 and references therein.
- [17] A. Fillos, S.S. Hefner, R. Tsu, *J. Vac. Sci. Technol. B* 14 (6) (1996) 3431.
- [18] Y. Kanemutsu, H. Uto, Y. Masumoto, T. Masumoto, T. Futagi, H. Mimura, *Phys. Rev. B* 48 (1993) 2827.
- [19] S. Guha, P. Steiner, W. Lang, *J. Appl. Phys.* 79 (1996) 8664.
- [20] Z. Iqbal, S. Veprek, *J. Phys. C: Solid State Phys.* 15 (1982) 377.
- [21] H. Tanino, A. Kuprin, H. Deai, N. Koshida, *Phys. Rev. B* 53 (1996) 1937.
- [22] Y. Gao, T. López-Ríos, *Solid State Commun.* 60 (1986) 55.
- [23] S. Hayashi, H. Abe, *Jpn. J. Appl. Phys.* 23 (1984) L824.
- [24] J. Fortner, J.S. Lannin, *Surf. Sci.* 254 (1991) 251.
- [25] G.A.N. Connel, R.J. Nemanich, C.C. Tsai, *Appl. Phys. Lett.* 36 (1980) 31.
- [26] W.S. Bacsá, J.S. Lannin, *Appl. Phys. Lett.* 61 (1992) 19.
- [27] J.C. Tsang, in: M. Cardona, G. Guntherodt (Eds.), *Light Scattering in Solids, Topics in Applied Physics, Vol. V*, Springer, Berlin, 1989, p. 233, chap. 6.
- [28] V.I. Merkulov, J.S. Lannin, J.M. Cowley, in: R.W. Collins (Ed.), *Advances in Microcrystalline and Nanocrystalline Semiconductors*, Materials Research Society Symposia Proceedings No. 452MRS, Pittsburgh, 1996, p. 225.
- [29] J.E. Smith Jr., M.H. Brodsky, B.L. Crowder, M.I. Nathan, A. Pinczuk, *Phys. Rev. Lett.* 26 (1971) 642.
- [30] J.S. Lannin, P.J. Carrol, *Philos. Mag.* 45 (1982) 155.
- [31] G. Nilson, G. Nelin, *Phys. Rev. B* 6 (1972) 3777.
- [32] J.S. Lannin, in: J.I. Pankove (Ed.), *Semiconductors and Semimetals*, 21(B), Academic Press, Orlando, 1984, p. 159.
- [33] P.Y. Yu, M. Cardona, *Fundamentals of Semiconductors*, Springer, Berlin, 1996, p. 103.
- [34] D. Bimberg, et al., in: O. Madelung, et al. (Eds.), *Numerical data and functional relationships in science and technology*, Landolt-Bornstein, New Series, Group III, Vol. 17i, Springer, Berlin, 1985, p. 5.
- [35] D. Bimberg, et al., in: O. Madelung, et al. (Eds.), *Numerical Data and Functional Relationships in Science And Technology*, Landolt-Bornstein, New Series, Group III, Vol. 17a, Springer, Berlin, 1982, p. 72.
- [36] I. Kaiser, N.H. Nickel, W. Fuhs, W. Pilz, *Phys. Rev. B* 58 (1998) R1718.
- [37] C. Trallero-Giner, A. Debernardi, M. Cardona, A.I. Ekimov, *Phys. Rev. B* 57 (1998) 4664.
- [38] T. Okada, T. Iwaki, K. Yamamoto, H. Kashara, K. Abe, *Solid State Commun.* 49 (1984) 809.
- [39] F. Kozlowski, P. Steiner, F. Lang, in: Z. Feng, R. Tsu (Eds.), *Porous Silicon*, World Scientific, Singapore, 1994, p. 149.
- [40] S. Hayashi, *Solid State Commun.* 56 (1985) 375.
- [41] G.P. Lopinski, J.S. Lannin, *Appl. Phys. Lett.* 69 (1996) 2400.
- [42] G.D. Cody, in: J.I. Pankove (Ed.), *Semiconductors and Semimetals*, Vol. 21B, Academic Press, Orlando, 1984, p. 11.